INSTITUTE OF PHYSICS PUBLISHING INVERSE PROBLEMS

Inverse Problems **20** (2004) 1–24 PII: S0266-5611(04)78114-9

Rapid three-dimensional inversion of multi-transmitter electromagnetic data using the spectral Lanczos decomposition method

Michael S Zhdanov[1] **and Alexey Chernyavskiy**

Department of Geology and Geophysics, University of Utah, Salt Lake City, UT 84112, USA

E-mail: mzhdanov@mines.utah.edu

Received 19 March 2004
Published XX August 2004
Online at stacks.iop.org/IP/20/1
doi:10.1088/0266-5611/20/0/000

Abstract

In this paper, we develop a new method of three-dimensional (3-D) inversion of multi-transmitter electromagnetic data. We apply the spectral Lanczos decomposition method (SLDM) in the framework of the localized quasi-linear inversion introduced by Zhdanov and Tartaras (2002 *Geophys. J. Int.* **148** 506–19). The SLDM makes it possible to find the regularized solution of the ill-posed inverse problem for all values of the regularization parameter α at once. As an illustration, we apply this technique for interpretation of the helicopter-borne electromagnetic (HEM) data over inhomogeneous geoelectrical structures, typical for mining exploration. This technique helps to accelerate HEM data inversion and provides a stable and focused image of the geoelectrical target. The new method and the corresponding computer code have been tested on synthetic data. The case history includes interpretation of HEM data collected by INCO Exploration in the Voisey's Bay area of Canada.

PACS number: 78A45

1. Introduction

The problem of three-dimensional (3-D) inversion of multi-transmitter electromagnetic (EM) data arises in different practical applications. One of these applications is the interpretation of the helicopter-borne electromagnetic (HEM) surveys which are widely used in mineral exploration. The main difficulties in modelling and interpreting multi-transmitter data are related to the fact that, for any new observation point, one has to solve the forward problem anew for the corresponding position of the moving transmitter. In this situation, even forward modelling of multi-transmitter data over inhomogeneous structures requires an enormous

[1] Author to whom correspondence should be addressed.

number of computations. That is why, until recently, the interpretation of HEM data, for example, was restricted to a simple 1-D inversion only.

Zhdanov and Tartaras [1] developed a new approach to the modelling and inversion of multi-source array electromagnetic data based on so-called localized quasi-linear (LQL) approximation. In the LQL approximation, the anomalous electric field inside the inhomogeneous region is represented as the product of the background (incident) field and an electrical reflectivity tensor $\hat{\boldsymbol{\lambda}}_L$. This tensor is assumed to be source-independent and slowly varying and, therefore, can be computed on a much coarser grid than the field itself. It was demonstrated by numerous modelling examples that the LQL approximation is easy to compute and very accurate [2, 3]. For the inverse problem, we use the LQL approximation to formulate a linear integral equation for a modified material property tensor $\hat{\mathbf{m}}$, which is also source independent and then is estimated from the data. The recovered values of the tensor $\hat{\mathbf{m}}$ are used to find the electrical reflectivity tensor $\hat{\boldsymbol{\lambda}}_L$ and the anomalous conductivity. In the framework of this approach, forward modelling and the inversion of multi-source data can be computed simultaneously for all different positions of the transmitters.

The developed method resembles inversion based on the extended Born approximation and multi-stage inversion algorithms that could be derived within its respective framework [4–9], but there are some important differences which have been carefully discussed in the previous publications [2, 10, 11]. In particular, the extended Born approximation also replaces the (unknown) total field inside the scatterer with a product of the incident field and a tensor, but this scattering tensor is defined explicitly through a weighted integral of the anomalous conductivity. In the LQL approximation, in contrast, the reflectivity tensor itself is determined by the solution of the optimization problem. In addition, the two-step linear inversion approach developed by Torres-Verdin and Habashy [7] is based on an analytical expression for the scattering tensor that depends explicitly on the selected model of the anomalous conductivity distribution. We do not specify the reflectivity tensor $\hat{\boldsymbol{\lambda}}_L$ before inversion, and we determine $\hat{\boldsymbol{\lambda}}_L$ as the result of linear inversion. Hence, our scheme consists of three steps: (i) determination of the modified material property tensor $\hat{\mathbf{m}}$, (ii) evaluation of the electrical reflectivity tensor $\hat{\boldsymbol{\lambda}}_L$ and (iii) determination of the anomalous conductivity from $\hat{\mathbf{m}}$ and $\hat{\boldsymbol{\lambda}}_L$.

The main goal of the present paper is to develop a new technique for fast LQL inversion which employs the spectral Lanczos decomposition method [2, 12–14]. The LQL inversion is an ill-posed problem, and its solution requires application of the corresponding regularization methods. One of the most critical elements of any regularization algorithm is a selection of the regularization parameter α describing the trade-off between the misfit and stabilizing functionals [15, 16]. The traditional approach to the solution of this problem is based on multiple inversions with different values of α and a subsequent search for an optimal regularization parameter. This approach is extremely time-consuming, especially for a 3-D EM inverse problem. We demonstrate in this paper for the LQL inversion that, *the SLDM makes it possible to find the regularized solution of the ill-posed inverse problem for all values of the regularization parameter α at once* [2]. This technique helps to accelerate HEM data inversion significantly and provides a stable and focused image of the geoelectrical target.

The new method and the corresponding computer code has been tested on synthetic data. We applied this technique for interpretation of the HEM data collected by INCO Exploration in the Voisey's Bay area of Canada.

2. Background of the localized quasi-linear inversion

For completeness, we begin our paper with the formulation of the basic principles of LQL inversion. The quasi-linear (QL) approximation [10] is based on the assumption that the

anomalous field $\mathbf{E}^a$ inside the inhomogeneous domain is linearly proportional to the background field $\mathbf{E}^b$ through some tensor $\hat{\boldsymbol{\lambda}}_L$:

$$\mathbf{E}^a(\mathbf{r}) \approx \hat{\boldsymbol{\lambda}}_L(\mathbf{r}) \cdot \mathbf{E}^b(\mathbf{r}). \tag{1}$$

In the framework of the localized quasi-linear (LQL) approximation [1, 2], it is assumed that the electrical reflectivity tensor $\hat{\boldsymbol{\lambda}}_L$ is source-independent.

Substituting formula (1) into the corresponding EM integral equations, we obtain integral representations for the LQL approximations of the anomalous electric, $\mathbf{E}^a_{LQL}(\mathbf{r}_j)$, and magnetic, $\mathbf{H}_{LQL}{}^a(\mathbf{r}_j)$, fields:

$$\begin{aligned}\mathbf{E}^a_{LQL}(\mathbf{r}_j) &\approx \int\int\int_D \widehat{\mathbf{G}}_E(\mathbf{r}_j \mid \mathbf{r}) \cdot \Delta\sigma(\mathbf{r})(\hat{\mathbf{I}} + \hat{\boldsymbol{\lambda}}_L(\mathbf{r})) \cdot \mathbf{E}^b(\mathbf{r})\, dv \\ &= \mathbf{G}_E[\Delta\sigma(\mathbf{r})(\hat{\mathbf{I}} + \hat{\boldsymbol{\lambda}}_L(\mathbf{r})) \cdot \mathbf{E}^b(\mathbf{r})], \end{aligned} \tag{2}$$

$$\begin{aligned}\mathbf{H}^a_{LQL}(\mathbf{r}_j) &\approx \int\int\int_D \widehat{\mathbf{G}}_H(\mathbf{r}_j \mid \mathbf{r}) \cdot \Delta\sigma(\mathbf{r})(\hat{\mathbf{I}} + \hat{\boldsymbol{\lambda}}_L(\mathbf{r})) \cdot \mathbf{E}^b(\mathbf{r})\, dv \\ &= \mathbf{G}_H[\Delta\sigma(\mathbf{r})(\hat{\mathbf{I}} + \hat{\boldsymbol{\lambda}}_L(\mathbf{r})) \cdot \mathbf{E}^b(\mathbf{r})], \end{aligned} \tag{3}$$

where $\mathbf{r}_j$ and $\mathbf{r}$ are the observation and integration points respectively, $\hat{\mathbf{I}}$ is the identity tensor, $\mathbf{G}_E$ and $\mathbf{G}_H$ are the corresponding Green's linear operators and $\widehat{\mathbf{G}}_E(\mathbf{r}_j \mid \mathbf{r})$ and $\widehat{\mathbf{G}}_H(\mathbf{r}_j \mid \mathbf{r})$ are the electric and magnetic Green's tensors defined for an unbounded conductive medium with a background conductivity σ_b.

Following Zhdanov and Fang [10] and Zhdanov and Tartaras [1], we introduce a new tensor function,

$$\hat{\mathbf{m}}(\mathbf{r}) = \Delta\sigma(\mathbf{r})(\hat{\mathbf{I}} + \hat{\boldsymbol{\lambda}}_L(\mathbf{r})), \tag{4}$$

which we call a modified material property tensor.

Equations (2) and (3) take the form

$$\mathbf{E}^a_{LQL}(\mathbf{r}_j) = \mathbf{G}_E[\hat{\mathbf{m}}(\mathbf{r}) \cdot \mathbf{E}^b(\mathbf{r})], \tag{5}$$

$$\mathbf{H}^a_{LQL}(\mathbf{r}_j) = \mathbf{G}_H[\hat{\mathbf{m}}(\mathbf{r}) \cdot \mathbf{E}^b(\mathbf{r})]. \tag{6}$$

Following Habashy *et al* [4], and Torres-Verdin and Habashy [6], we can take into account that the Green's tensor $\widehat{\mathbf{G}}_E(\mathbf{r}_j \mid \mathbf{r})$ exhibits either singularity or a peak at the point where $\mathbf{r}_j = \mathbf{r}$. Therefore, the dominant contribution to the integral $\mathbf{G}_E[\hat{\mathbf{m}}(\mathbf{r}) \cdot \mathbf{E}^b(\mathbf{r})]$ in equation (5) is from some vicinity of point $\mathbf{r}_j = \mathbf{r}$. Assuming also that the background field $\mathbf{E}^b(\mathbf{r})$ is slowly varying within domain D, we can rewrite equation (5) as

$$\mathbf{E}^a_{LQL}(\mathbf{r}_j) \approx \mathbf{G}_E[\hat{\mathbf{m}}(\mathbf{r})] \cdot \mathbf{E}^b(\mathbf{r}_j), \tag{7}$$

where the tensor Green's operator $\mathbf{G}_E[\hat{\mathbf{m}}(\mathbf{r})]$ is given by the formula

$$\mathbf{G}_E[\hat{\mathbf{m}}(\mathbf{r})] = \int\int\int_D \widehat{\mathbf{G}}_E(\mathbf{r}_j \mid \mathbf{r}) \cdot \hat{\mathbf{m}}(\mathbf{r})\, dv. \tag{8}$$

Comparing equations (1) and (7), we find that

$$\mathbf{E}^a_{LQL}(\mathbf{r}_j) \approx \hat{\boldsymbol{\lambda}}_L(\mathbf{r}_j) \cdot \mathbf{E}^b(\mathbf{r}_j) \approx \mathbf{G}_E[\hat{\mathbf{m}}(\mathbf{r})] \cdot \mathbf{E}^b(\mathbf{r}_j).$$

Therefore, the electrical reflectivity tensor can be determined from the solution of the minimization problem,

$$\|\hat{\boldsymbol{\lambda}}_L(\mathbf{r}_j) \cdot \mathbf{E}^b(\mathbf{r}_j) - \mathbf{G}_E[\hat{\mathbf{m}}(\mathbf{r})] \cdot \mathbf{E}^b(\mathbf{r}_j)\|_{L_2(D)} = \min. \tag{9}$$

Noting that

$$\|\hat{\boldsymbol{\lambda}}_L(\mathbf{r}_j) \cdot \mathbf{E}^b(\mathbf{r}_j) - \mathbf{G}_E[\hat{\mathbf{m}}(\mathbf{r})] \cdot \mathbf{E}^b(\mathbf{r}_j)\|_{L_2(D)} \leqslant \|\hat{\boldsymbol{\lambda}}_L(\mathbf{r}_j) - \mathbf{G}_E[\hat{\mathbf{m}}(\mathbf{r})]\|_{L_2(D)} \|\mathbf{E}^b(\mathbf{r}_j)\|_{L_2(D)},$$

we can substitute another problem,

$$\|\hat{\boldsymbol{\lambda}}_L(\mathbf{r}_j) - \mathbf{G}_E[\hat{\mathbf{m}}(\mathbf{r})]\|_{L_2(D)} = \min \tag{10}$$

for the minimization problem (9).

The solution of equation (11) gives us *a localized electrical reflectivity tensor* $\hat{\boldsymbol{\lambda}}_L(\mathbf{r})$, which is obviously source-independent.

Note that, in the framework of the LQL method, we can choose different forms of the reflectivity tensor. For example, we can introduce a scalar or diagonal reflectivity tensor. The choice of electrical reflectivity tensor is related to the physics of the problem and the accuracy and speed required in the computations. The interested reader can find the detailed analysis of the selection of the different types of electrical reflectivity tensor and related accuracy of the LQL approximation in Zhdanov and Tartaras [1].

We assume now that the anomalous parts of the electric, $\mathbf{E}^a(\mathbf{r}_j)$, and/or magnetic, $\mathbf{H}^a(\mathbf{r}_j)$, fields (generated by a transmitter with one or different positions) are measured at a number of observation points, $\mathbf{r}_j$. Using the LQL approximations (5) and (6) for the observed fields, $\mathbf{d}$, we arrive at the following equation:

$$\mathbf{d} = \mathbf{G}_d[\hat{\mathbf{m}}(\mathbf{r}) \cdot \mathbf{E}^b(\mathbf{r})], \tag{11}$$

which is linear with respect to the material property tensor $\hat{\mathbf{m}}(\mathbf{r})$. In the last equation, $\mathbf{d}$ stands for the electric or magnetic field, $\mathbf{E}$ or $\mathbf{H}$, and $\mathbf{G}_d$ denotes the Green's operators $\mathbf{G}_E$ or $\mathbf{G}_H$ respectively.

We can solve the linear equation (11) with respect to $\hat{\mathbf{m}}(\mathbf{r})$, which is source-independent. Now, a reflectivity tensor $\hat{\boldsymbol{\lambda}}_L(\mathbf{r})$ is determined, based on the condition (11), which constitutes an important step of the LQL inversion. This problem is solved by a standard least-squares optimization.

Knowing $\hat{\boldsymbol{\lambda}}_L(\mathbf{r})$ and $\hat{\mathbf{m}}(\mathbf{r})$, we can find $\Delta\sigma(\mathbf{r})$ from equation (4). Note that, in a general case, equation (4) should hold for any frequency, because the electrical reflectivity and the material property tensors are the functions of frequency as well: $\hat{\boldsymbol{\lambda}}_L = \hat{\boldsymbol{\lambda}}_L(\mathbf{r}, \omega)$, $\hat{\mathbf{m}} = \hat{\mathbf{m}}(\mathbf{r}, \omega)$. In reality, of course, it holds only approximately. Therefore, the conductivity, $\Delta\sigma(\mathbf{r})$, can be found by using the least-squares method of solving equation (4):

$$\|\hat{\mathbf{m}}(\mathbf{r}, \omega) - \Delta\sigma(\mathbf{r})(\hat{\mathbf{I}} + \hat{\boldsymbol{\lambda}}_L(\mathbf{r}, \omega))\|_{L_2(\omega)} = \min. \tag{12}$$

This inversion scheme can be used for a multi-source technique, because $\hat{\boldsymbol{\lambda}}_L$ and $\hat{\mathbf{m}}$ are source-independent. It reduces the original nonlinear inverse problem to three linear inverse problems: the first (quasi-Born inversion) for tensor $\hat{\mathbf{m}}$, another for tensor $\hat{\boldsymbol{\lambda}}_L$, and the third (correction of the result of the quasi-Born inversion) for the conductivity $\Delta\sigma$.

We can rewrite equation (11) using matrix notations:

$$\mathbf{d} = \mathbf{G}\mathbf{m}. \tag{13}$$

Here $\mathbf{m}$ is the vector-column of the modified material property tensor $\hat{\mathbf{m}}$, $\mathbf{d}$ is the vector-column of the field data, and the matrix $\mathbf{G}$ is the matrix of the linear operator defined by formula (11).

The solution of the inverse problem is reduced to the inversion of linear system (13) with respect to $\mathbf{m}$ and then to computing $\hat{\boldsymbol{\lambda}}_L$ using condition (10). After that, we find $\Delta\sigma$ as a least-squares solution of the optimization problem (12). Note that in the case of a single-frequency observations, we still have to solve the optimization problem (12), if we consider the full electrical reflectivity and material property tensors. In a case of single-frequency observations and a scalar electrical reflectivity tensor, optimization problem (12) is reduced to a simple algebraic equation.

3. The Tikhonov regularization method

Zhdanov and Tartaras [1] used the re-weighted regularized conjugate gradient method with image focusing [17] for solving the system of the linear equations (13). In this paper, we will apply another numerical technique, the spectral Lanczos decomposition method (SLDM), to solve this problem. We will demonstrate that the SLDM technique makes it possible to find the regularized solution of the ill-posed inverse problem for all values of the regularization parameter α at once, thus providing an effective tool for optimal α selection.

Let us consider first the general approach to linear inverse problem solution, based on the Tikhonov regularization technique [2]. We introduce the following parametric functional:

$$P^{\alpha}(\mathbf{m}, \mathbf{d}) = \|\mathbf{W}_d\mathbf{G}\mathbf{m} - \mathbf{W}_d\mathbf{d}\|^2 + \alpha\|\mathbf{W}_m\mathbf{m} - \mathbf{W}_m\mathbf{m}_{apr}\|^2, \tag{14}$$

where $\mathbf{W}_d$ and $\mathbf{W}_m$ are some real weighting matrices of data and model parameters; $\mathbf{m}_{apr}$ is some *a priori* model and $\|\ldots\|$ denotes the Euclidean norm in the spaces of data and models. To avoid the numerical imbalance between the constituent norms, the proper normalization of the functionals of equation (14) is achieved by the appropriate selection of the weighting matrices, and/or by the appropriate selection of the regularization parameter α, which will be discussed later.

In the majority of practical applications, we assume that $\mathbf{W}_m = \mathbf{I}$ (where $\mathbf{I}$ is the identity matrix), but it also can be chosen arbitrarily, for example, as a matrix of first- or second-order finite-difference differentiation to obtain a smooth solution. In particular, it was demonstrated in [2] that the recommended choice of the model parameter weighting matrix $\mathbf{W}_m$ is the square root of the integrated sensitivity matrix according to

$$\mathbf{W}_m = \mathrm{diag}(\mathbf{F}^*\mathbf{F})^{1/4} = \mathrm{diag}(\mathbf{G}^*\mathbf{G})^{1/4}, \tag{15}$$

where $\mathbf{F}$ is the Frechet derivative matrix, which is equal to matrix $\mathbf{G}$ for the linear inverse problem, and the asterisk $*$ denotes a transposed complex conjugate matrix.

Following Zhdanov [2], we will solve our problem in the space of weighted parameters. We introduce a vector of weighted model parameters:

$$\mathbf{m}_w = \mathbf{W}_m\mathbf{m}.$$

The original vector of model parameters is given by the inverse transformation

$$\mathbf{m} = \mathbf{W}_m^{-1}\mathbf{m}_w.$$

We also introduce a weighted forward operator:

$$\mathbf{G}_w = \mathbf{G}\mathbf{W}_m^{-1}.$$

Now we can rewrite the functional $P^{\alpha}(\mathbf{m}_w, \mathbf{d})$ with matrix notations:

$$\begin{aligned} P^{\alpha}(\mathbf{m}_w, \mathbf{d}) = {} & (\mathbf{W}_d^*\mathbf{G}_w^*\mathbf{m}_w^* - \mathbf{W}_d^*\mathbf{d}^*)(\mathbf{W}_d\mathbf{G}_w\mathbf{m}_w - \mathbf{W}_d\mathbf{d}) \\ & + \alpha(\mathbf{m}_w^* - \mathbf{m}_{w,apr}^*)(\mathbf{m}_w - \mathbf{m}_{w,apr}). \end{aligned}$$

According to the basic principles of the regularization method, we have to find a quasi-solution of the inverse problem as the model $\mathbf{m}_{w,\alpha}$ minimizing the parametric functional

$$P^{\alpha}(\mathbf{m}_{w,\alpha}, \mathbf{d}) = \min.$$

The solution of this problem can be found from the corresponding regularized normal equation as [2] (p 75)

$$\mathbf{m}_{w,\alpha} = [\mathbf{G}_w^*\mathbf{W}_d^2\mathbf{G}_w + \alpha\mathbf{I}]^{-1}[\mathbf{G}_w^*\mathbf{W}_d^2\mathbf{d} + \alpha\mathbf{m}_{w,apr}]. \tag{16}$$

The regularization parameter α describes the trade-off between the best fitting and most reasonable stabilization. In a case where α is selected to be too small, the minimization of the parametric functional $P^{\alpha}(\mathbf{m})$ is equivalent to the minimization of the misfit functional; therefore we have no regularization, which can result in an unstable incorrect solution. When α is too large, the minimization of the parametric functional $P^{\alpha}(\mathbf{m})$ is equivalent to the minimization of the stabilizing functional $s(\mathbf{m})$, which will force the solution to be closer to the *a priori* model. Ultimately, we would expect the final model to be exactly like the *a priori* model, while the observed data are totally ignored in the inversion. Thus, the critical question in the regularized solution of the inverse problem is the selection of the optimal regularization parameter α. The basic principles used for determining the regularization parameter α are discussed in Tikhonov and Arsenin [15]. According to the pioneering work of Tikhonov, the optimal value of the regularization parameter α is determined from the misfit condition

$$\|\mathbf{W}_d\mathbf{G}_w\mathbf{m}_{w,\alpha} - \mathbf{W}_d\mathbf{d}\| = \delta, \tag{17}$$

where δ is some *a priori* estimation of the level of the 'weighted' noise of the data:

$$\|\mathbf{W}_d\delta\mathbf{d}\| = \delta. \tag{18}$$

A simple numerical method for determining the parameter α is based on a progression of numbers:

$$\alpha_k = \alpha_1 q^{k-1}, \qquad k = 1, 2, \ldots, n, \quad 0 < q < 1. \tag{19}$$

For any number α_k, we can find the element $\mathbf{m}_{\alpha_k}$ minimizing $P^{\alpha_k}(\mathbf{m}_{w,\alpha_k}, \mathbf{d})$ and calculate the misfit $\varphi(\alpha_k)$:

$$\varphi(\alpha_k) = \|\mathbf{W}_d\mathbf{G}_w\mathbf{m}_{w,\alpha_k} - \mathbf{W}_d\mathbf{d}\|^2.$$

It is proven in regularization theory that $\varphi(\alpha_k)$ is a monotonic and not increasing function of k [2, 15]. The quasi-optimal value of the parameter α is the number $\alpha_{Tikhonov} = \alpha_{k0}$, for which, with the necessary accuracy, we have the equality (17).

Hansen [16] introduced an alternative method for determining the parameter α based on the L-curve analysis. It represents a simple graphical tool for qualitative selection of the quasi-optimal regularization parameter. The L-curve method is based on plotting for all possible α, the curve of the stabilizing functional, $s(\alpha)$ versus the misfit functional, $\varphi(\alpha)$. The L-curve illustrates the trade-off between the best fitting (minimizing a misfit) and most reasonable stabilization (minimizing a stabilizer). In a case where α is selected to be too small, the minimization of the parametric functional P^{α} is equivalent to the minimization of the misfit functional; therefore $\varphi(\alpha)$ decreases while $s(\alpha)$ increases. When α is too large, the minimization of the parametric functional P^{α} is equivalent to the minimization of the stabilizing functional; therefore $s(\alpha)$ decreases, while $\varphi(\alpha)$ increases. The distinct corner, separating the vertical and the horizontal branches of this curve, corresponds to the quasi-optimal value of the regularization parameter $\alpha_{L\text{-}curve}$.

The advantage of the L-curve method over the Tikhonov criterion is that the former does not require any information about the level of noise in the data, while the Tikhonov's misfit condition (17) explicitly uses this information. The disadvantage is that there is no rigorous proof of the existence of the distinct corner in the L-curve, which sometimes is difficult to find.

Both methods, however, have a clear practical limitation, because they require a complete numerical solution of the inverse problem for multiple values of the regularization parameter α, which is extremely time consuming, especially for a 3-D EM inverse problem with multi-transmitter data. We will demonstrate in the next section that application of the spectral Lanczos decomposition method (SLDM) makes it possible to overcome this limitation, because

it delivers the regularized solution of the ill-posed inverse problem for all values of the regularization parameter α at once [2]. This is one of the most important advantages of the SLDM method over other solvers in regularized inversion.

4. Application of the SLDM for solving the linear system of equations for the LQL method

One can see that expression (16) contains a matrix inversion. The SLDM provides an effective tool for matrix inversion. It is especially suitable for the regularized inversion, because it can be applied only once for all different values of the regularization parameter α [2].

Introducing notations

$$\mathbf{c} = \mathbf{G}_{\mathbf{w}}^{*}\mathbf{W}_{\mathbf{d}}^{\mathbf{2}}\mathbf{d} \quad \text{and} \quad \mathbf{B} = \mathbf{G}_{\mathbf{w}}^{*}\mathbf{W}_{\mathbf{d}}^{\mathbf{2}}\mathbf{G}_{w}, \tag{20}$$

and assuming that $\mathbf{m}_{w,apr} = 0$, we can rewrite equation (16) in the form

$$\mathbf{m}_{w,\alpha} = (\mathbf{B} + \alpha\mathbf{I})^{-1}\mathbf{c}. \tag{21}$$

Denoting by f_α the function

$$f_\alpha(\mathbf{B}) = (\mathbf{B} + \alpha\mathbf{I})^{-1},$$

we obtain

$$\mathbf{m}_{w,\alpha} = f_\alpha(\mathbf{B})\mathbf{c}. \tag{22}$$

Thus, we have arrived at the problem of computing a function of the matrix $\mathbf{B}$. This problem can be solved by the SLDM outlined in an appendix.

First, we apply the Lanczos algorithm (43) for QT decomposition of matrix $\mathbf{B}$

$$\beta_0 = 1, \qquad \mathbf{q}_0 = 0, \qquad \mathbf{q}_1 = \mathbf{c}/\|\mathbf{c}\|, \tag{23a}$$

$$\text{while } \beta_j \neq 0, \qquad \mathbf{q}_{j+1} = \mathbf{r}_j/\beta_j, \qquad \alpha_j\mathbf{I} = \mathbf{q}_j^{\mathrm{T}}\mathbf{B}\mathbf{q}_j, \tag{23b}$$

$$\mathbf{r}_j = (\mathbf{B} - \alpha_{\mathbf{j}}\mathbf{I}_{\mathbf{N}})\mathbf{q}_j - \beta_{j-1}\mathbf{q}_{j-1}, \qquad \beta_j = \|\mathbf{r}_j\|, \quad j = 1, 2, \ldots, N-1, \tag{23c}$$

where I_N is $N \times N$ identity matrix and superscript T denotes transposition.

As the result, we find an orthogonal matrix, $\mathbf{Q}_L$, and a tri-diagonal matrix, $\mathbf{T}_L$, where L is an iteration step of the Lanczos algorithm. Finally, we arrive at the following formula for regularized solution:

$$\mathbf{m}_{w,\alpha} = \|\mathbf{c}\|\mathbf{Q}_L f_\alpha(\mathbf{T}_L)\mathbf{e}_1^{(L)} = \|\mathbf{c}\|\mathbf{Q}_L(\mathbf{T}_L + \alpha\mathbf{I})^{-1}\mathbf{e}_1^{(L)}, \tag{24}$$

where $\mathbf{e}_1^{(L)}$ is the unit vector of the order L: $\mathbf{e}_1^{(L)} = (1, 0, 0, \ldots, 0)$. The advantage is that now we have to run the Lanczos algorithm only once for all different values of the regularization parameter α. After that we have to invert only a tri-diagonal matrix $(\mathbf{T}_L + \alpha\mathbf{W}_m^2)$ for a different α, which is a much simpler operation.

The misfit condition (17) can be rewritten now in the form

$$\|\mathbf{W}_d\mathbf{G}_w\|\mathbf{c}\|\mathbf{Q}_L(\mathbf{T}_L + \alpha\mathbf{I})^{-1}\mathbf{e}_1^{(L)} - \mathbf{W}_d\mathbf{d}\| = \delta. \tag{25}$$

5. Re-weighted linear inversion

5.1. The Tikhonov parametric functional with a pseudo-quadratic stabilizer

The parametric functional (14) contains the minimum norm stabilizing functional, which, as a rule, provides a smooth solution. The smooth solutions for geoelectrical structures have difficulties, however, in describing the sharp geoelectrical boundaries between different geological formations. This problem arises, for example, in inversion for the local resistive or conductive target with sharp boundaries between the resistor/conductor and the host rocks, which is a typical model in mining exploration. The mathematical technique for solving this problem was described in a monograph by Zhdanov [2]. It is based on introducing a special type of stabilizing functional, the so-called minimum support or minimum gradient support functionals [17]. We call this technique a focusing regularized inversion to distinguish it from the traditional smooth regularized inversion. Note that there exists, actually, a family of different stabilizing functionals, selecting the classes of inverse models with different properties [2] (p 45). For example, an approach based on the total variation (TV) method for reconstructing an image with sharp boundaries has been introduced by Rudin *et al* [18]. However, it was demonstrated in Portniaguine and Zhdanov [17] that in geophysical inversion the minimum support and minimum gradient support functionals produce better results than the TV method.

In general cases, a stabilizing functional can be represented in the form of the pseudo-quadratic functional:

$$s(\mathbf{m}) = (W_e\mathbf{m}, W_e\mathbf{m}), \tag{26}$$

where operator W_e is a linear operator of multiplication of the model parameters function $m(\mathbf{r})$ by the function $w_e(\mathbf{r})$, which depends on m. For discrete model parameters, using matrix notations, operator W_e can be expressed as the matrix multiplication

$$W_e\mathbf{m} = \mathbf{W}_e\mathbf{m}, \tag{27}$$

where diagonal matrix $\mathbf{W}_e$ is computed differently for different stabilizers.

In the case of the minimum support functional, we have [2] (p 156)

$$\mathbf{W}_e = \operatorname{diag}\left[\frac{1}{(|m|^2 + e^2)^{1/2}}\right], \tag{28}$$

where e is a small number.

Once again, we introduce the vector of the weighted model parameters in the form

$$\mathbf{m}_{e,w} = \mathbf{W}_e\mathbf{W}_m\mathbf{m},$$

where matrix $\mathbf{W}_e$ is the focusing matrix which depends on $\mathbf{m}$, and $\mathbf{W}_m$ is a conventional model parameters weighting matrix.

Once it is obtained, the initial model parameter will be given by the inverse transformation

$$\mathbf{m} = \mathbf{W}_e^{-1}\mathbf{W}_m^{-1}\mathbf{m}_{e,w}.$$

We also introduce a weighted forward operator,

$$\mathbf{G}_{e,w} = \mathbf{G}\mathbf{W}_m^{-1}\mathbf{W}_e^{-1}.$$

The corresponding parametric functional can be written as

$$P^{\alpha}(\mathbf{m}_{e,w}, \mathbf{d}) = (\mathbf{W}_d^*\mathbf{G}_{e,w}\mathbf{m}_{e,w}^* - \mathbf{W}_d\mathbf{d}^*)(\mathbf{W}_d\mathbf{G}_{e,w}\mathbf{m}_{e,w} - \mathbf{W}_d\mathbf{d}) + \alpha(\mathbf{m}_{e,w}^* - \mathbf{m}_{w,apr}^*)(\mathbf{m}_{e,w} - \mathbf{m}_{w,apr}). \tag{29}$$

Therefore, the problem of the minimization of the parametric functional introduced by equation (29) can be treated in a similar way to the minimization of the conventional Tikhonov functional. The only difference is that now we introduce some variable weighting matrix $\mathbf{W}_e$ for the model parameters. The minimization problem for the parametric functional introduced by equation (29) can be solved using the ideas of the traditional least-squares method.

5.2. The Lanczos algorithm with re-weighting

The regularized solution of the corresponding normal equation for the minimization problem of functional (29) has the form

$$\mathbf{m}_{e,w,\alpha} = [\mathbf{G}^*_{e,w}\mathbf{W}^2_d\mathbf{G}_{e,w} + \alpha\mathbf{I}]^{-1}[\mathbf{G}^*_{e,w}\mathbf{W}^2_d\mathbf{d} + \alpha\mathbf{m}_{w,apr}]. \tag{30}$$

Introducing notations

$$\mathbf{c} = \mathbf{G}^*_{\mathbf{e,w}}\mathbf{W}^{\mathbf{2}}_{\mathbf{d}}\mathbf{d} \quad \text{and} \quad \mathbf{B} = \mathbf{G}^*_{e,w}\mathbf{W}^2_d\mathbf{G}_{e,w}, \tag{31}$$

and assuming that $\mathbf{m}_{w,apr} = 0$, we can rewrite this equation in the form

$$\mathbf{m}_{e,w,\alpha} = (\mathbf{B} + \alpha\mathbf{I})^{-1}\mathbf{c}. \tag{32}$$

Applying the Lanczos algorithm, we arrive at the following formula for the regularized solution:

$$\mathbf{m}_{e,w,\alpha(L)} = \|\mathbf{c}\|\mathbf{Q}_L f_\alpha(\mathbf{T}_L)\mathbf{e}^{(L)}_1 = \|\mathbf{c}\|\mathbf{Q}_L(\mathbf{T}_L + \alpha\mathbf{I})^{-1}\mathbf{e}^{(L)}_1. \tag{33}$$

First, we can apply the truncated Lanczos algorithm with $L = L_1$ to obtain an initial truncated solution, $\mathbf{m}_{e,w,\alpha(1)}$. Using formula (28), we compute the focusing matrix $\mathbf{W}_{e(1)}$ for this initial model:

$$\mathbf{W}_{e(1)} = \operatorname{diag}\left[\frac{1}{(|m_w|^2_{\alpha(1)} + e^2)^{1/2}}\right]. \tag{34}$$

Then we run the Lanczos algorithm (33) with this matrix. We analyse the misfit behaviour for a number of truncated solutions again (with the fixed matrix $\mathbf{W}_{e(1)}$), and terminate the process when the misfit has stabilized. For this model $\mathbf{m}_{\alpha(2)}$ we can find a new focusing matrix, $\mathbf{W}^2_{e2}$, and apply the same Lanczos algorithm (28) with the new matrix:

$$\mathbf{W}_{e(2)} = \operatorname{diag}\left[\frac{1}{(|m|^2_{\alpha(12)} + e^2)^{1/2}}\right].$$

This process can be repeated several times, until the required degree of focusing is achieved.

6. 3-D LQL inversion of synthetic HEM data

One of the most important possible applications of the LQL inversion technique is the interpretation of frequency-domain helicopter-borne data. This type of airborne survey is used extensively in mining exploration. We use the integral equation code SYSEM [19] to simulate such a survey over a conductive (200 Ω m) cubical body located in a resistive (5000 Ω m) half-space. Figure 1 depicts a 3-D view of the model. Five lines were flown over the target at an altitude of 30 m and at a distance of 25 m from each other. A schematic planview of the survey is shown in figure 2.

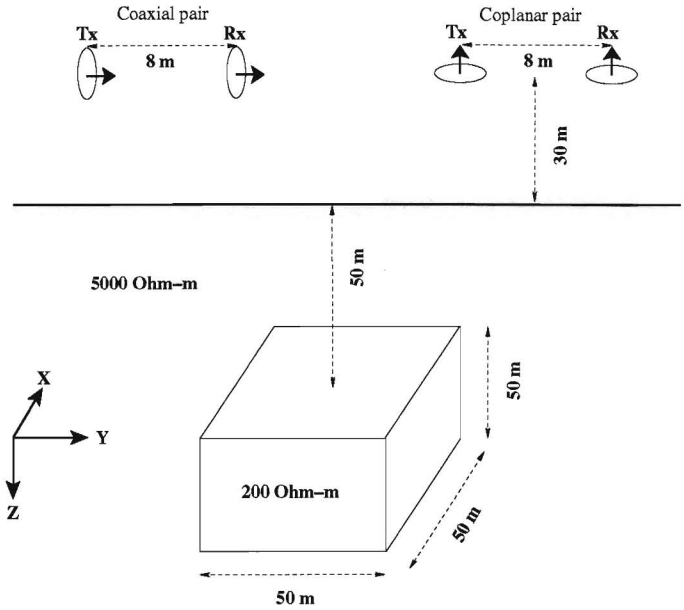

Figure 1. Schematic view of a conductive cubical body located within a resistive half-space. Frequencies used for HEM survey are 900 and 7200 Hz.

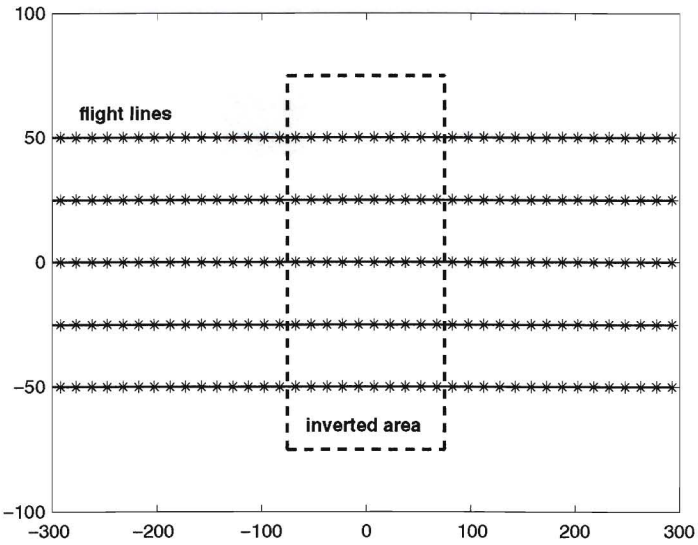

Figure 2. Schematic planview of a model HEM survey comprising of five flight lines.

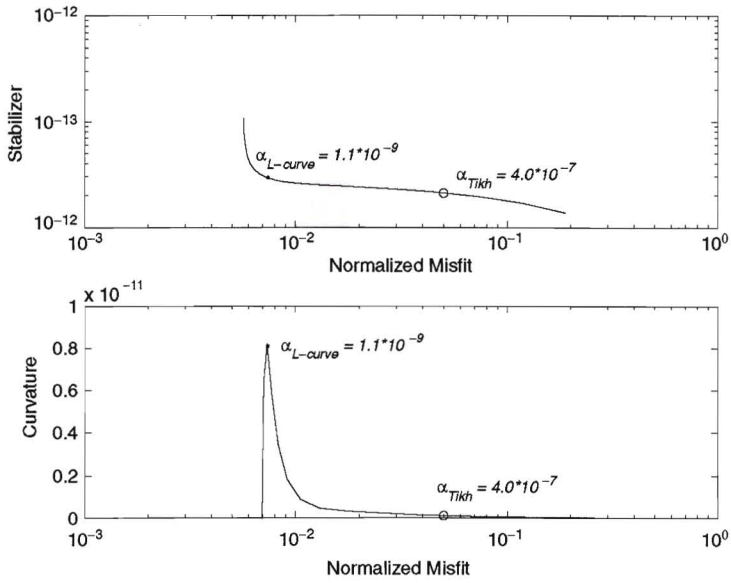

Figure 3. L-curve (upper panel) and its curvature (lower panel) for model study. The corner of the L-curve is shown by a point. It corresponds to the maximum of the curvature. For comparison, we show by a circle the point on the L-curve corresponding to Tikhonov's quasi-optimal value of $\alpha_{Tikhonov}$ obtained using the misfit condition.

The moving transmitter–receiver system was a pair of vertical magnetic dipoles (simulating a horizontal coplanar coil pair) and a pair of horizontal magnetic dipoles (simulating a vertical coaxial coil pair) with 8 m horizontal separation. The *yy* (coaxial) and *zz* (coplanar) components of the anomalous magnetic field were measured every 15 m along the lines (50 observation points in each line). Two frequencies were used: 900 Hz and 7.2 kHz.

We added 2% random noise to the anomalous magnetic field and then inverted it using the SLDM method. The area of inversion, centred around the body, was 150 m $\times$ 150 m $\times$ 150 m and was divided into 12 $\times$ 12 $\times$ 12 cells.

The advantage of the SLDM method is that we can find the regularized solution for several different values of the regularization parameter α with practically no additional computational cost. Hence, this method is very well suited for applying the L-curve analysis [16], which is based on plotting for all possible α, the curve of the stabilizing functional, $s(\alpha)$ versus the misfit functional, $\varphi(\alpha)$ (see figure 3, upper panel). The distinct corner, separating the vertical and the horizontal branches of this curve, corresponds to the quasi-optimal value of the regularization parameter $\alpha_{L\text{-}curve}$, which is equal to 1.1×10^{-9} in this case. This point is clearly seen in the L-curve curvature plot by a local maximum (figure 3, lower panel). For comparison, we show by a circle the point on the L-curve corresponding to Tikhonov's quasi-optimal value of $\alpha_{Tikhonov}$ obtained using the misfit condition. Note that the inversions run with $\alpha_{L\text{-}curve}$ and $\alpha_{Tikhonov}$ values of the regularization parameter produce practically the same results. We present here both techniques for optimal regularization parameter selection (the Tikhonov approach and the L-curve method) to illustrate the computational power of the SLDM method. Indeed, the SLDM allows us to determine the stabilizing functional, $s(\alpha)$, and

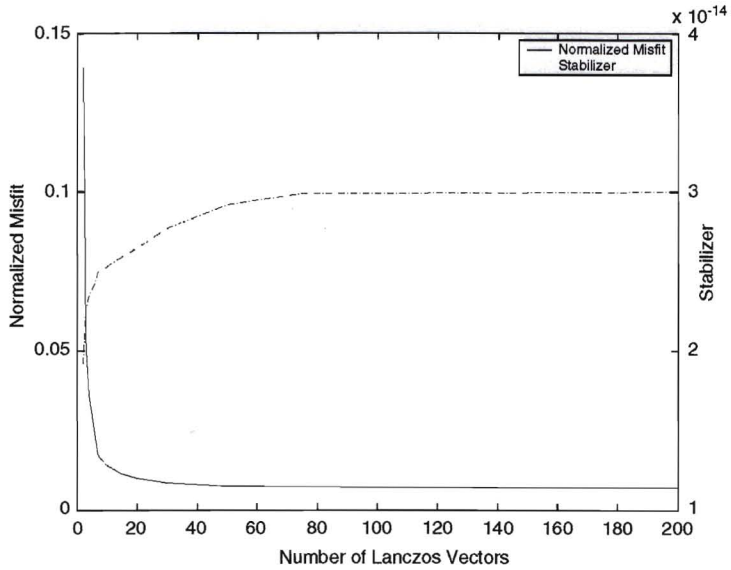

Figure 4. Dependence of normalized misfit and stabilizer on the number of Lanczos vectors used in inversion. One can see that the misfit converges very fast and becomes less than 2% just after 30 Lanczos steps.

the misfit functional, $\varphi(\alpha)$, for any value of the regularization parameter α practically without any additional computational cost!

Figure 4 shows the behaviour of the normalized misfit and stabilizer as the functions of the steps L of the truncated Lanczos algorithm. One can see that the misfit converges very fast and becomes less than 2% just after 30 Lanczos steps.

Figure 5 shows the vertical cross-sections of the 3-D model obtained as the result of inversion with Tikhonov's quasi-optimal value of the regularization parameter. We have chosen Tikhonov's criterion, because we know the noise level of the synthetic data. The image is slightly unfocused because this image is generated with the minimum norm stabilizer. We use this smooth model to compute the focusing matrix $\mathbf{W}_{e(1)}$ according to formula (34). After that we apply the SLDM algorithm again. The new image is shown in figure 6. Both the location and the shape of the conductive body are determined very well. These results demonstrate the stability of the method in the presence of noise (results of inversion of noise-free data, not shown here, are very similar). Moreover, the truncated SLDM algorithm is extremely fast. The 3-D inversion for 250 total different transmitter–receiver pairs requires 6 s of CPU time on an Athlon 1000 MHz processor.

7. LQL inversion of HEM data collected in the Voisey's Bay area

We have used our method to invert real HEM data collected by INCO Exploration in the Voisey's Bay area in Canada. This area is characterized by high-conductivity Ni–Cu sulphide deposits hosted by resistive troctolite dikes [20]. A geological map of the area with several identified deposits is shown in figure 7. We applied the 3-D inversion to the HEM data within

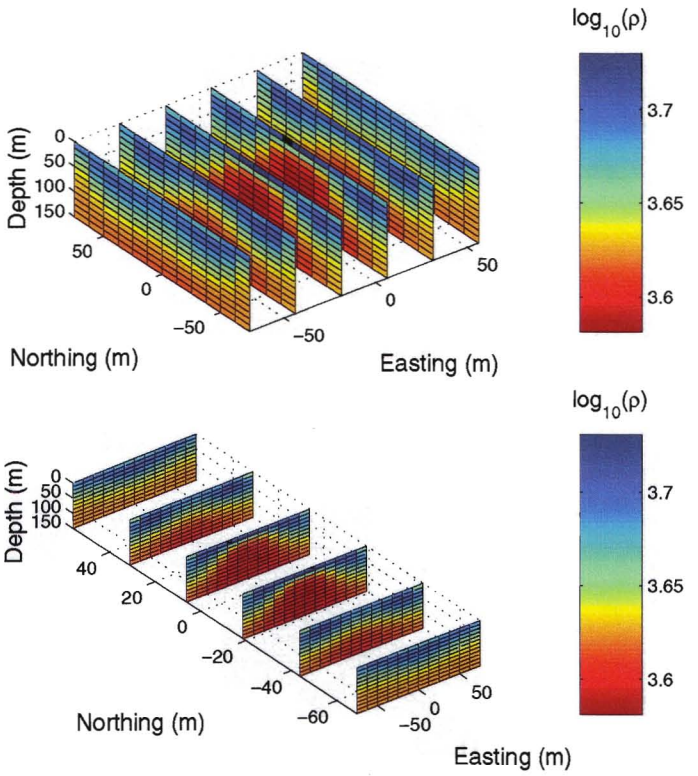

Figure 5. Cross-sections of the inverse model obtained by the smooth inversion of synthetic data.

two areas outlined in figure 7. One of these areas (no. 1) corresponds to the location of the Ovoid deposit, which is a flat-lying deposit of very high conductance, and comprises 70% massive sulphide [21]. Area No. 2 is associated with another prospective mineralization zone, adjacent to Area No. 1.

Based on drilling information, incorporated into figure 7, we have assumed a 20 m deep, conductive overburden with a resistivity of 10 Ω m. We used the coaxial components from the lowest frequency (900 Hz) because they are the least sensitive to the presence of the conductive overburden. The data were first interpolated along a uniform (in each direction) grid and then transformed from ppm (part per million of the primary magnetic field in the free air) to anomalous field values, assuming a uniform background resistivity beneath the overburden of 1900 Ω m. The data comprise parts of four flight lines, at a distance of 200 m from each other. The area of inversion was 700 m × 600 m × 160 m and was divided into 14 × 30 × 8 cells. Figure 8 presents the L-curve, computed for the different values of the regularization parameter α. We chose the quasi-optimal $\alpha = 6.3 \times 10^{-16}$ according to the Tikhonov misfit condition, because it corresponds to the known level of noise in the observed data (norm square of noise is estimated as of 3%). Figure 9 describes the behaviour of the normalized misfit and stabilizer as the functions of the steps L of the truncated Lanczos algorithm. One can see that both functions converge very fast, and misfit becomes less than 3% just after eight Lanczos steps.

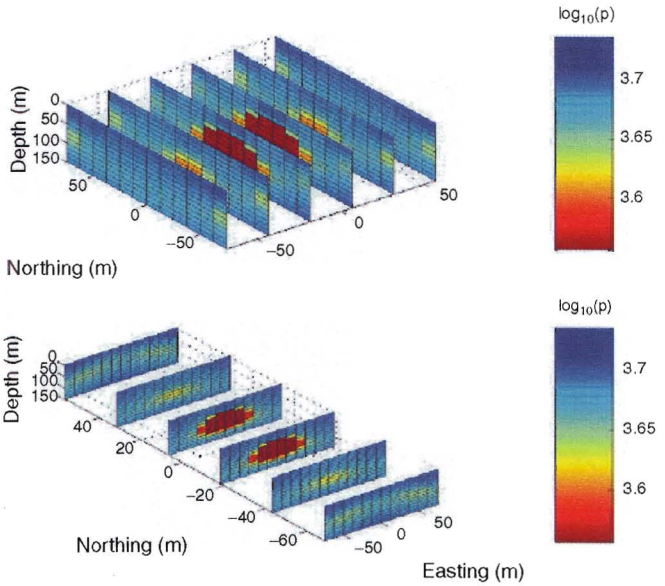

Figure 6. Cross-sections of the inverse model generated by the focusing inversion.

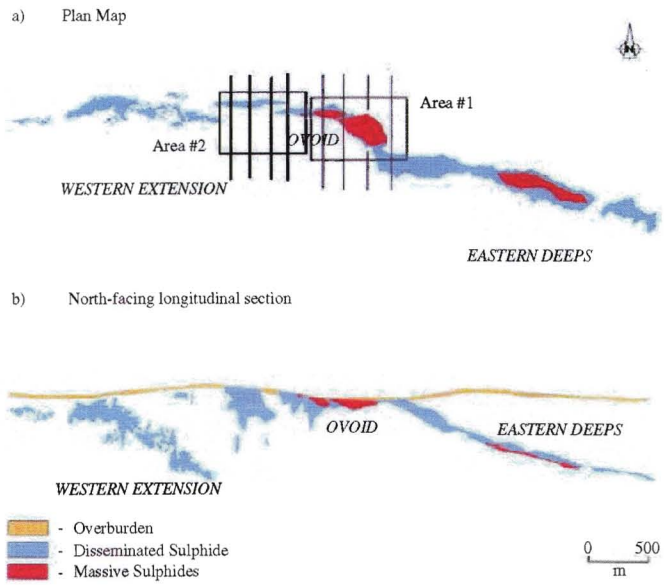

Figure 7. A map of the Voisey's Bay sulphide deposits. The data measured along eight flight lines flown over two areas were used for inversion.

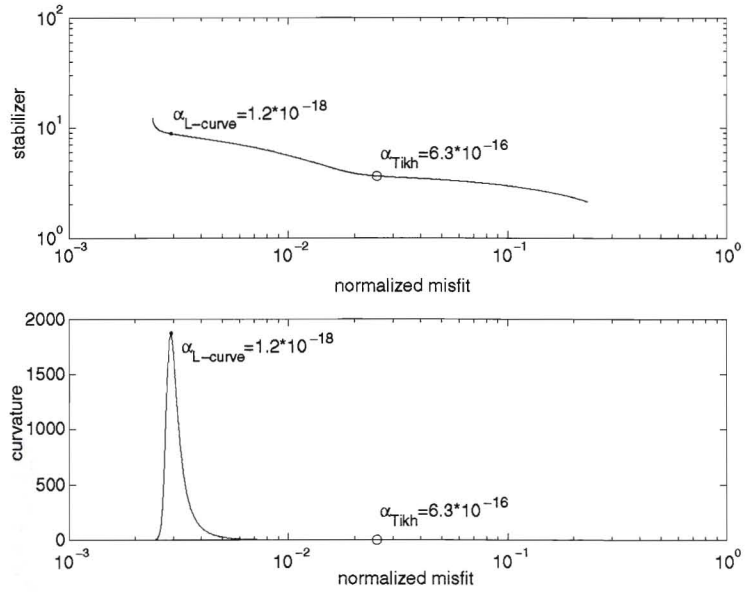

Figure 8. L-curve and its curvature for inversion of HEM data from Area no. 1. The corner of the L-curve is shown by a point. For comparison, we show by a circle the point on the L-curve corresponding to Tikhonov's quasi-optimal value of $\alpha_{Tikhonov}$ obtained using the misfit condition.

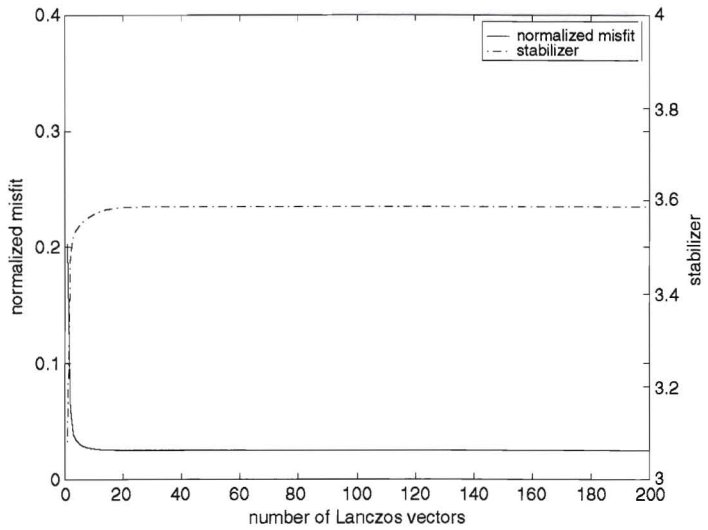

Figure 9. A dependence of the normalized misfit and stabilizer on the number of the Lanczos vectors used in inversion. The misfit converges very fast and becomes less than 3% just after eight Lanczos steps.

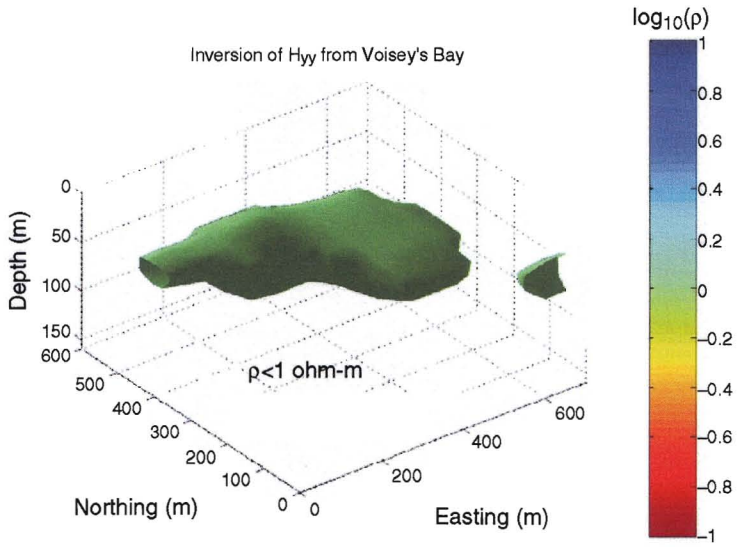

Figure 10. A volume rendering of a 3-D resistivity image obtained after the inversion of the coaxial components measured over Area no. 1. The cut-off value for the resistivity is 1 Ωm.

Figure 10 shows a 3-D image of the inversion result for the coaxial components. Only values of resistivity below a threshold of 1 Ω m have been plotted out of the cube-shaped area of inversion. Figure 11 presents the same result in the form of vertical slices through the model generated as a result of the inversion. Figure 12 shows the observed and predicted data along all four flight lines. The observed data are shown by the dotted curve. The inversion results obtained by 'full' SLDM comprised of 200 Lanczos steps, are shown by solid lines, while the dashed lines correspond to the truncated SLDM with only 25 Lanczos steps. One can see that the agreement between all three curves is very good.

The results seem reasonable and in good agreement with the existing information about the Ovoid deposit, and with the inversion result obtained by Zhdanov and Tartaras [1] using the conjugate gradient method.

LQL inversion based on the SLDM method was also applied to the HEM data collected in Area no. 2 (see figure 7). We used the data collected along four flight lines, at a distance of 200 m from each other. The area of inversion has the same dimensions as the previous one, 700 m × 600 m × 160 m, and is divided into 14 × 30 × 8 cells. Figure 13 presents the L-curve, computed for the different values of the regularization parameter α. In this case, we chose the quasi-optimal $\alpha = 7.6 \times 10^{-17}$ according to the Tikhonov misfit condition, because it corresponds to the known level of noise in the observed data (norm square of noise is estimated at 3%). The behaviour of the normalized misfit and stabilizer as the functions of the steps L of the truncated Lanczos algorithm is shown in figure 14. This figure illustrates a rapid convergence of both functions with the normalized misfit equal to less than 3% just after 40 Lanczos steps.

Figure 15 shows a 3-D image of the inversion result for the coaxial components. Figure 16 presents the same result in the form of vertical slices through the model generated as a result of the inversion. Figure 17 shows the observed and predicted data along all four flight lines.

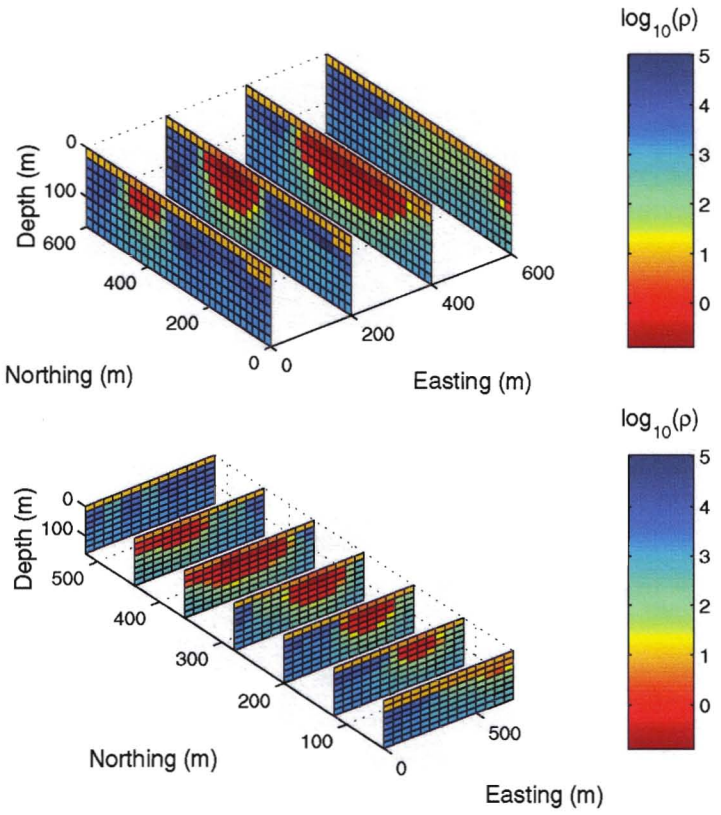

Figure 11. Cross-sections of 3-D resistivity distribution obtained after inversion of HEM data from Area no. 1.

The observed data are shown by the dotted curve. The inversion results obtained by the 'full' SLDM algorithm comprised of 200 Lanczos steps are shown by solid lines, while the dashed lines correspond to the truncated SLDM method with only 26 Lanczos steps. Once again, the agreement between all three curves is very good.

Note that, for comparison, we obtained an inverse model which corresponds to the $\alpha = 7.3 \times 10^{-19}$ selected based on L-curve criterion (the point of the maximum curvature of the L-curve is shown in figure 13, lower panel). The resulting inverse model was practically the same as the one shown in figures 15 and 16.

The successful application of the LQL inversion to real HEM data in a complex geological environment with large resistivity contrasts shows that the method can be an effective tool for fast 3-D inversion of helicopter-borne electromagnetic data (see figure 18). AQ1

8. Conclusions

We have developed a new efficient method of 3-D multi-transmitter data inversion based on the LQL approximation. We have used the spectral Lanczos decomposition for fast and accurate

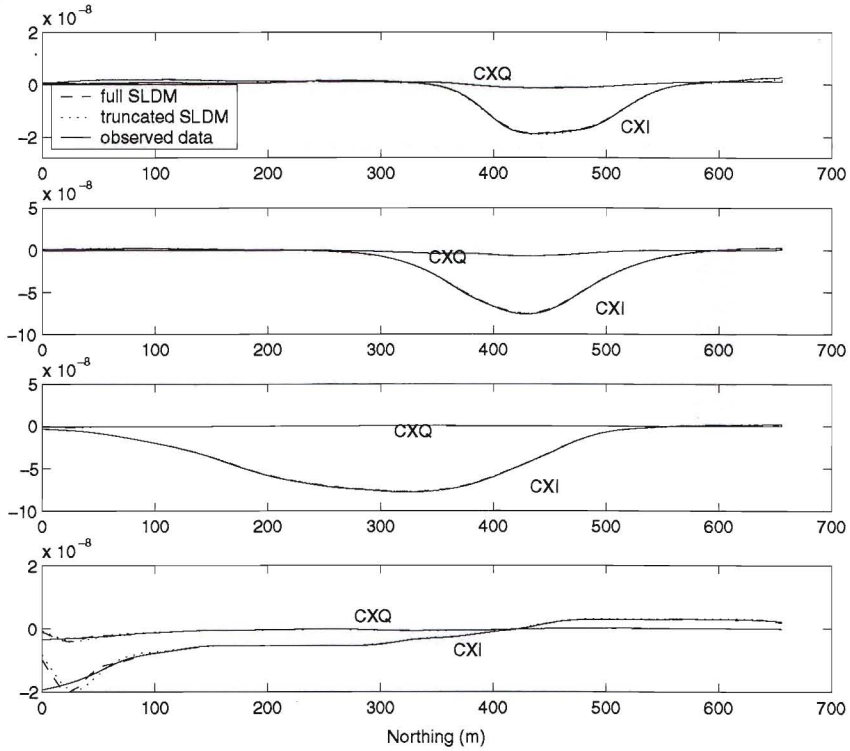

Figure 12. The magnetic field values along four North–South lines in Area no. 1. The real and imaginary components of the observed field (marked by CXI-coaxial inphase and CXQ-coaxial quadrature indices) are shown along with the predicted field obtained by the 'full' and truncated SLDM.

inversion of synthetic data simulating a helicopter-borne survey over a conductive body. The Lanczos decomposition has demonstrated its special usefulness for inversion with multiple regularization parameter values, especially when the noise level is not known implicitly. The obtained results demonstrate that this new technique helps to accelerate multi-transmitter data inversion and provides a stable and focused image of the geoelectrical target.

We also inverted a real HEM dataset provided by INCO Exploration. The results successfully locate the shallow massive sulphide deposits and show that the LQL and Lanczos methods work well together in real, complex geological environments. The numerical experiments on synthetic models as well as successful inversion of real data make the LQL approximation along with SLDM a prominent technique in multi-source data inversion.

Acknowledgments

The authors acknowledge the support of the University of Utah Consortium for Electromagnetic Modeling and Inversion (CEMI), which includes Baker Atlas Logging Services, BHP Billiton World Exploration Inc., Electromagnetic Instruments Inc., ExxonMobil Upstream

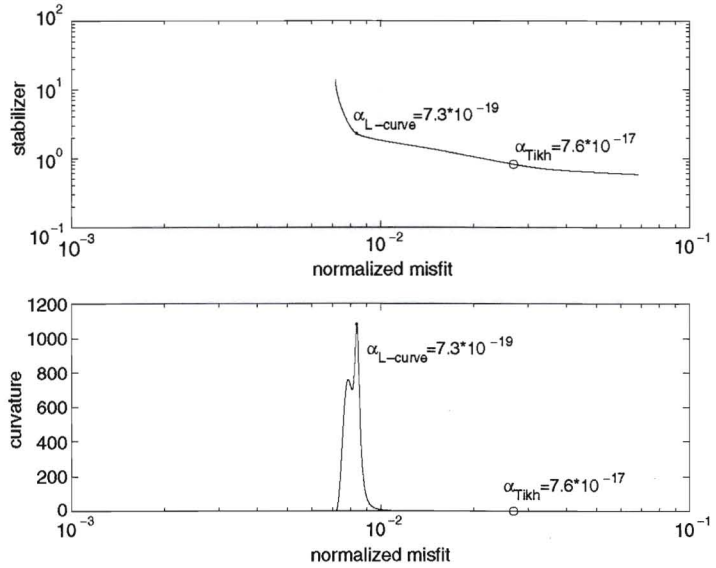

Figure 13. L-curve and its curvature for inversion of HEM data from Area no. 2. The corner of the L-curve is shown by a point. For comparison, we show by a circle the point on the L-curve corresponding to Tikhonov's quasi-optimal value of $\alpha_{Tikhonov}$ obtained using the misfit condition. The corner of the L-curve is shown by a dot.

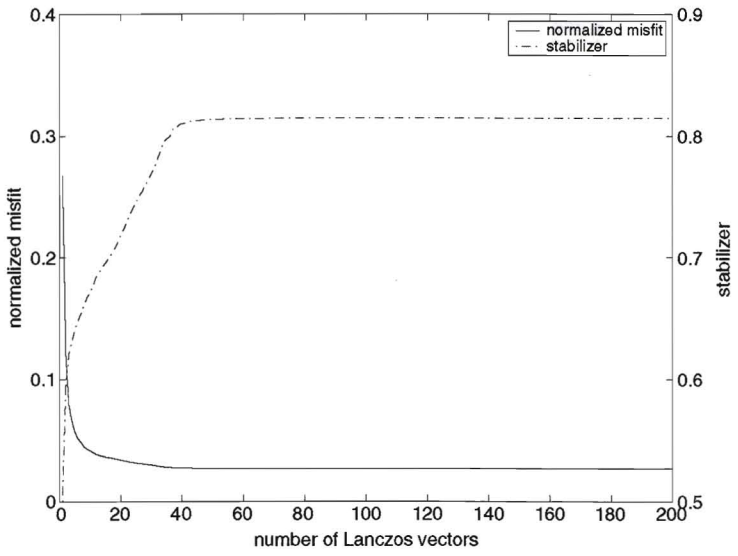

Figure 14. A dependence of the normalized misfit and stabilizer on the number of the Lanczos vectors used in inversion. The normalized misfit becomes less than 3% just after 40 Lanczos steps.

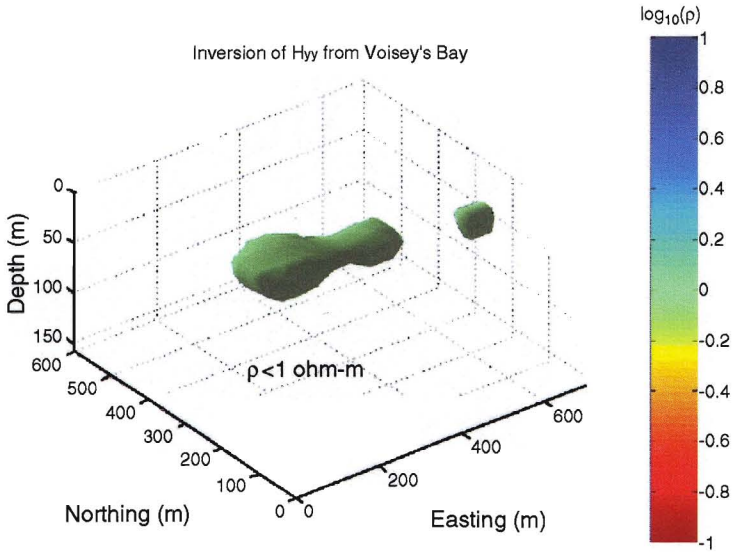

Figure 15. A volume rendering of a 3-D resistivity image obtained after the inversion of the coaxial components measured over Area no. 2. The cut-off value for the resistivity is 1 Ωm.

Research Company, INCO Exploration, International Energy Services Inc., Naval Research Laboratory, Rio Tinto-Kennecott, Shell International Exploration and Production Inc., Schlumberger Oilfield Services, and Sumitomo Metal Mining Co.

We also thank INCO Exploration, and particularly Dr A King, for providing us with the HEM data set.

We are thankful to the Guest Editors of this Special Issue of *Inverse Problems* for their thoughtful comments and recommendations, which helped to improve the paper.

Appendix. The spectral Lanczos decomposition method

The most appropriate technique for solving a large, symmetric eigenproblem $\mathbf{Av} = \lambda\mathbf{v}$ is delivered by the Lanczos method [13]. This method involves partial tridiagonalization of the given matrix. One advantage of the Lanczos method is that the estimation of the extremal eigenvalues appears even before the tridiagonalization is complete. This makes the Lanczos method extremely useful in practical applications [12, 14]. We will outline the basic principles of the Lanczos method following the monograph of Zhdanov [2].

The Lanczos method is based on generating the orthonormal basis in Krylov space $K_L = \text{span}\{\mathbf{c}, \mathbf{Ac}, \ldots, \mathbf{A}^{L-1}\mathbf{c}\}$ by applying the Gram–Schmidt orthogonalization process. In matrix notations, this approach is associated with the reduction of the symmetric matrix $\mathbf{A}$ to a tridiagonal matrix $\mathbf{T}_L$ and also with the special properties of $\mathbf{T}_L$. This reduction (called also QT decomposition) is described by the formula

$$\mathbf{Q}_L^{\mathrm{T}}\mathbf{A}\mathbf{Q}_L = \mathbf{T}_L, \tag{A.1}$$

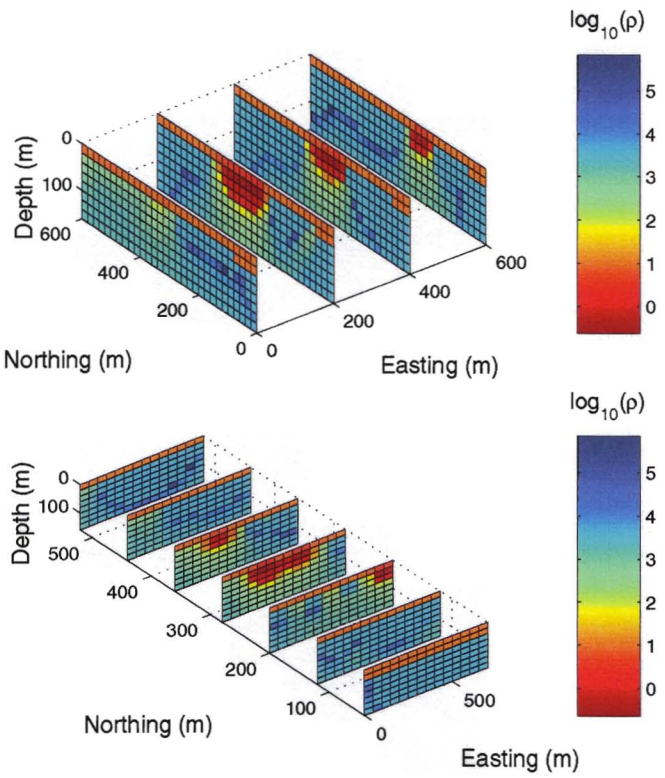

Figure 16. Cross-sections of the resistivity distribution obtained after inversion of the HEM data from Area no. 2.

where $\mathbf{T}_L$ is the tri-diagonal symmetric matrix

$$\mathbf{T}_L = \begin{bmatrix} \alpha_1 & \beta_1 & \dots & 0 \\ \beta_1 & \alpha_2 & \beta_2 & \\ \vdots & & & \vdots \\ 0 & & \beta_{L-1} & \alpha_L \end{bmatrix},$$

$\mathbf{Q}_L$ is the matrix of the orthogonal basis of Krylov space

$$\mathbf{Q}_L = [\mathbf{q}_1, \mathbf{q}_2, \dots, \mathbf{q}_L],$$

and $\mathbf{Q}_L^{\mathrm{T}}$ is the transpose of $\mathbf{Q}_L$. Vectors $\mathbf{q}_j$ of the basis are called *Lanczos vectors*. All Lanczos vectors are N-vectors, consisting of N scalar components. It is assumed also that

$$\beta_j > 0, \quad j = 1, 2, \dots, L-1. \tag{A.2}$$

We consider first the tridiagonalization process using Krylov space of dimension N: $K_N = \mathrm{span}\{\mathbf{c}, \mathbf{Ac}, \dots, \mathbf{A}^{N-1}\mathbf{c}\}$. In this case, according to the definition, the matrix $\mathbf{Q}_N$ is orthogonal, $\mathbf{Q}_N^{\mathrm{T}} = \mathbf{Q}_N^{-1}$. Therefore, the reduction formula (A.1) can be rewritten as

$$\mathbf{AQ}_N = \mathbf{Q}_N \mathbf{T}_N. \tag{A.3}$$

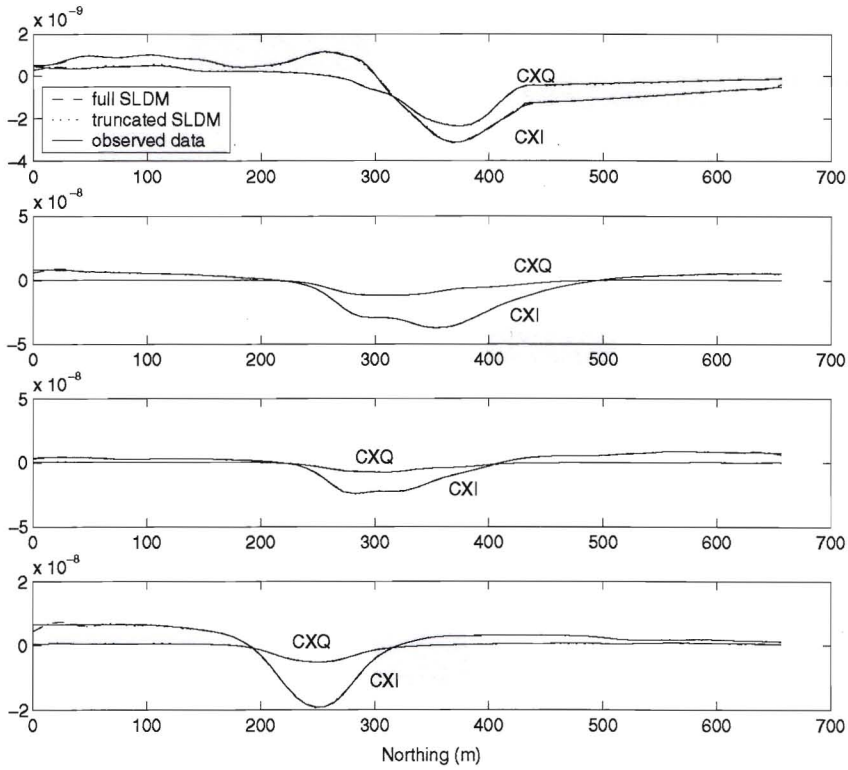

Figure 17. The magnetic field values along four North–South lines in Area no. 2. The real and imaginary components of the observed field (marked by CXI-coaxial inphase and CXQ-coaxial quadrature indices) are shown along with the predicted field obtained by 'full' and truncated SLDM.

For example, equating the jth column of each side of (A.3), we obtain a recursive formula

$$\beta_j \mathbf{q}_{j+1} = \mathbf{A}\mathbf{q}_j - \beta_{j-1}\mathbf{q}_{j-1} - \alpha_j \mathbf{q}_j = \mathbf{r}_j, \tag{A.4}$$

which holds for $j = 1, \ldots, N$, if we define $\beta_0 \mathbf{q}_0 = \beta_N \mathbf{q}_N = 0$.

The orthogonality of $\mathbf{Q}_N$ can be written in the form $\mathbf{q}_i^{\mathrm{T}} \mathbf{q}_j = \delta_{ij}$, where δ_{ij} is Kronecker's delta symbol. Therefore, multiplying (A.4) by $\mathbf{q}_j^{\mathrm{T}}$, we obtain

$$0 = \mathbf{q}_j^{\mathrm{T}} \mathbf{A}\mathbf{q}_j - \alpha_j \mathbf{I}_N$$

or

$$\alpha_j \mathbf{I}_N = \mathbf{q}_j^{\mathrm{T}} \mathbf{A}\mathbf{q}_j, \quad j = 1, 2, \ldots, N-1, \tag{A.5}$$

where $\mathbf{I}_N$ is the $N \times N$ identity matrix.

Also, using (A.2) and the orthogonality of $\mathbf{Q}_N$, we have

$$\beta_j = \|\beta_j \mathbf{q}_{j+1}\| = \|\mathbf{r}_j\|. \tag{A.6}$$

From equation (A.4), we also obtain

$$\mathbf{q}_{j+1} = \frac{\mathbf{r}_j}{\beta_j}, \quad j = 1, 2, \ldots, N-1. \tag{A.7}$$

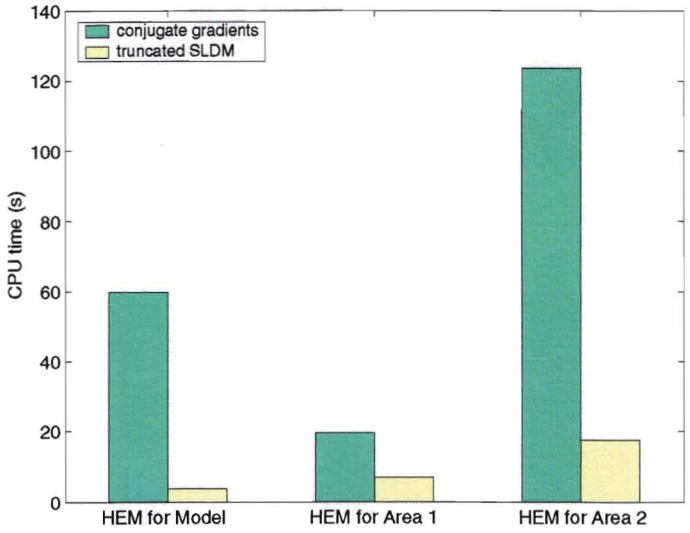

Figure 18. A comparison of CPU time needed for inversion using conjugate gradients method and truncated spectral Lanczos decomposition. The computations were conducted on an AMD Athlon 1000 MHz processor.

Thus, we have formulated the Lanczos algorithm to determine $\alpha_j, \mathbf{r}_j, \beta_j$ and $\mathbf{q}_{j+1}$ from the given values of $\mathbf{q}_{j-1}$, $\mathbf{q}_j$ and β_{j-1}, assuming that

$$\beta_0 \mathbf{q}_0 = 0, \qquad \mathbf{q}_1 = \frac{\mathbf{c}}{\|\mathbf{c}\|} \quad \text{and} \quad \beta_j > 0. \tag{A.8}$$

The Lanczos algorithm can be summarized as follows:

$$\beta_0 = 1, \qquad \mathbf{q}_0 = 0, \qquad \mathbf{q}_1 = \mathbf{c}/\|\mathbf{c}\|, \tag{A.9a}$$

$$\text{while } \beta_j \neq 0, \qquad \mathbf{q}_{j+1} = \mathbf{r}_j/\beta_j, \qquad \alpha_j \mathbf{I} = \mathbf{q}_j^{\mathrm{T}} \mathbf{A} \mathbf{q}_j, \tag{A.9b}$$

$$\mathbf{r}_j = (\mathbf{A} - \alpha_j \mathbf{I}_N)\mathbf{q}_j - \beta_{j-1}\mathbf{q}_{j-1}, \qquad \beta_j = \|\mathbf{r}_j\|, \quad j = 1, 2, \ldots, N-1. \tag{A.9c}$$

As a result of the Lanczos algorithm we obtain matrices $\mathbf{Q}_N$ and $\mathbf{T}_N$. Note that, in general cases, we can run the Lanczos algorithm until $j = L-1$, where $L < N$. In this case we obtain $L \times L$ matrices $\mathbf{Q}_L$ and $\mathbf{T}_L$, which can still be effectively used to evaluate the eigenvalues and eigenvectors of the original matrix $\mathbf{A}$ [13].

In many practical situations, we have to compute a vector

$$\mathbf{d} = f(\mathbf{A})\mathbf{c}, \tag{A.10}$$

where $\mathbf{A}$ is a symmetric square $N \times N$ matrix, f is a function defined on a spectral interval of $\mathbf{A}$, and $\mathbf{c}, \mathbf{d}$ are vectors defined in Euclidean space E_N. The Lanczos algorithm makes it possible to solve this problem using the QT decomposition and the following formula:

$$\mathbf{d} = \|\mathbf{c}\| \mathbf{Q}_N f(\mathbf{T}_N) \mathbf{e}_1^{(N)}, \tag{A.11}$$

where $\mathbf{e}_1^{(N)}$ is the unit vector of the order N:

$$\mathbf{e}_1^{(N)} = (1, 0, \ldots, 0, \ldots, 0).$$

Thus, we reduce the original problem of calculating the function f of matrix $\mathbf{A}$ to a much smaller problem of calculating the same function of the tridiagonal matrix $\mathbf{T}_N$. In many practical cases this problem can be easily solved numerically.

Note that we can use L steps of the Lanczos method to generate matrices $\mathbf{Q}_L$ and $\mathbf{T}_L$, $L < N$, and to introduce a natural approximation to vector $\mathbf{d}$ as

$$\mathbf{d}_L = \|\mathbf{c}\|\mathbf{Q}_L f(\mathbf{T}_L)\mathbf{e}_1^{(L)}. \tag{A.12}$$

References

[1] Zhdanov M and Tartaras E 2002 Inversion of multi-transmitter 3-D electromagnetic data based on the localized quasi-linear approximation *Geophys. J. Int.* **148** 506–19

[2] Zhdanov M 2002 *Geophysical Inverse Theory and Regularization Problems* (Amsterdam: North-Holland/American Elsevier) p 609

[3] Zhdanov M, Tartaras E and Gribenko A 2004 Fast 3D imaging from a single borehole using tensor induction logging data *Petrophysics* **45** 167–78

[4] Habashy T M, Groom R W and Spies B R 1993 Beyond the Born and Rytov approximations: a nonlinear approach to electromagnetic scattering *J. Geophys. Res.* **98** 1759–75

[5] Habashy T M, Oristaglio M L and de Hoop A T 1994 Simultaneous nonlinear reconstruction of two-dimensional permittivity and conductivity *Radio Sci. Fast Forward Inverse Scattering Meth.* **29** 1101–18

[6] Torres-Verdin C and Habashy T M 1994 Rapid 2.5-dimensional forward modeling and inversion via a new scattering approximation *Radio Sci.* **29** 1051–79

[7] Torres-Verdin C and Habashy T M 1995 A two-step linear inversion of two-dimensional electrical conductivity *IEEE Trans. Antennas Propagation* **43** 405–15

[8] Reis Dos D, Lambert M and Lesselier D 2001 On the modeling and inversion of 3-D inclusions in conductive media using extended Born models in the diffusive regime *Int. J. Appl. Electromagn. Mech.* **14** 477–81

[9] Reis Dos D, Lambert M and Lesselier D 2002 Extended Born domain integral models of diffusive fields *IEEE Trans. Magn.* **2** 577–80

[10] Zhdanov M and Fang S 1996 Quasi-linear approximation in 3D EM modeling *Geophysics* **61** 646–65
Zhdanov M and Fang S 1996 3-D quasi-linear electromagnetic inversion *Radio Sci.* **31** 741–54

AQ2 [11] Zhdanov M and Fang S 1999 3D quasi-linear electromagnetic modeling and inversion *Three Dimensional Electromagn. SEG Monograph* 233–55

[12] Druskin V and Knizhnerman L 1994 Spectral approach to solving three-dimensional Maxwell's diffusion equations in the time and frequency domains *Radio Sci.* **29** 937–53

[13] Golub G H and Van Loan C F 1996 *Matrix Computations* 3rd edn (Baltimore: The Johns Hopkins University Press) p 694

[14] Druskin V, Knizhnerman L and Lee P 1999 New spectral Lanczos decomposition method for induction modeling in arbitrary 3D geometry *Geophysics* **64** 701–6

AQ3 [15] Tikhonov A N and Arsenin V Y 1977 *Solution of Ill-posed Problems* (V H Winston and Sons) p 258

[16] Hansen C 1998 *Rank-deficient and Discrete Ill-posed Problems. Numerical Aspects of Linear Inversion* (Department of Mathematical Modeling, Technical University of Denmark, Lyngby) p 247

[17] Portniaguine O and Zhdanov M 1999 Focusing geophysical inversion images *Geophysics* **64** 874–87

[18] Rudin L I, Osher S and Fatemi E 1992 Nonlinear total variation based noise removal algorithms *Physica* D **60** 259–68

[19] Xiong Z 1992 EM modeling of three-dimensional structures by the method of system iteration using integral equations *Geophysics* **57** 1556–61

[20] Naldrett A J, Keats H, Sparkes K and Moore S 1996 Geology of the Voisey's Bay Ni–Cu–Co deposit, Labrador, Canada *Explor. Mining Geol.* **5** 169–79

AQ4 [21] Balch S J 2000 Ni–Cu sulphide deposits with examples from Voisey's Bay *Geophysics in Mineral Exploration: Fundamentals and Case Histories* p 21

AQ5 [22] Zhdanov M and Keller G 1994 *The Geoelectrical Methods in Geophysical Exploration* (Amsterdam: North-Holland/American Elsevier) p 900

Author Queries:

AQ1: Please check citation of figure 18.
AQ2: Provide volume number for reference [11].
AQ3: Provide place of publication for reference [15].
AQ4: Provide editors name, publisher and place for reference [21].
AQ5: Reference [22] is not cited. Please check.